molecular pharmaceutics

ARTICLE

pubs.acs.org/molecularpharmaceutics

The Involvement of Organic Anion Transporting Polypeptide in the Hepatic Uptake of Telmisartan in Rats: PET Studies with [^{11}C]Telmisartan

Tadayuki Takashima,*[,†] Yoshinobu Hashizume,[†] Yumiko Katayama,[†] Machiko Murai,[†] Yasuhiro Wada,[†] Kazuya Maeda,[‡] Yuichi Sugiyama,[‡] and Yasuyoshi Watanabe[†]

[†]RIKEN Center for Molecular Imaging Science, 6-7-3 Minatojima-minamimachi, Chuo-ku, Kobe, Hyogo 650-0047, Japan

[‡]Laboratory of Molecular Pharmacokinetics, Graduate School of Pharmaceutical Sciences, The University of Tokyo, 7-3-1 Hongo, Bunkyo-ku, Tokyo 113-0033, Japan

ABSTRACT: Telmisartan, a selective angiotensin II receptor antagonist, is primarily excreted via hepatobiliary transport. The predominant contribution of organic anion transporting polypeptide (OATP) 1B3 in its hepatic uptake of telmisartan has been demonstrated by in vitro transport studies. In the present study, a quantitative positron emission tomography (PET) methodology was developed for in vivo kinetic assessment of hepatobiliary transport of telmisartan. Serial abdominal PET scans were performed in rats following intravenous administration of [^{11}C]telmisartan as a radiotracer. PET scans revealed that [^{11}C]telmisartan was localized primarily in the liver and some of the radioactivity moved to the intestine, which corresponds to biliary excretion. Radiometabolite analysis by radiometric HPLC showed that [^{11}C]telmisartan was converted to its acylglucuronide, which was mainly detected in bile, but little in plasma and liver. Integration plot analysis revealed that [^{11}C]telmisartan was taken up into the liver as rapidly as the hepatic blood flow rate, and the radiometabolite was subsequently excreted into the bile. When rifampicin, a typical Oatp inhibitor, was coadministered with [^{11}C]telmisartan in rats, hepatic uptake clearance of [^{11}C]telmisartan was significantly decreased, whereas biliary efflux clearance was not changed. Coinjection with unlabeled telmisartan (4 and 10 mg/kg) also decreased hepatic uptake clearance of [^{11}C]telmisartan. On the other hand, PET imaging analysis revealed a significant increase of biliary efflux when telmisartan dose was increased to more than 4 mg/kg. These results suggested that the hepatic uptake of [^{11}C]telmisartan mainly consists of a saturable process mediated by Oatps in rats, according to noninvasive real-time measurement of tissue radioactivity with the use of PET. The present study with rats is expected to provide the feasibility of PET imaging study to quantitatively estimate OATP1B3 function in humans.

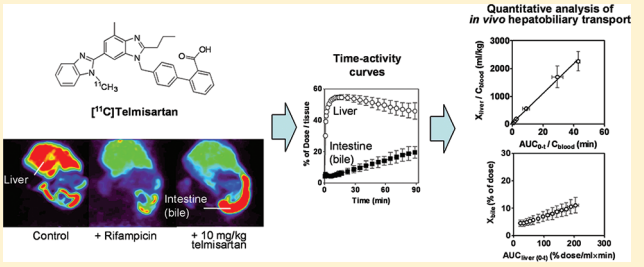

KEYWORDS: OATP/Oatp (organic anion transporting polypeptide), positron emission tomography (PET), hepatobiliary transport, telmisartan

INTRODUCTION

Telmisartan is a selective angiotensin II type 1 receptor blocker, which belongs to the group of angiotensin II receptor antagonists, resulting in a decrease of blood pressure. Telmisartan is metabolized to a pharmacologically inactive acylglucuronide by UDP-glucuronosyltransferases in the liver and intestine, and then the acylglucuronide is rapidly excreted into the bile.[1,2] Telmisartan is selectively distributed to the liver in rats,[3] and more than 98% of the total radioactivity is recovered in feces after intravenous administration of [^{14}C]telmisartan. The pharmacokinetic profile of telmisartan shows large interindividual variability, and also shows nonlinearity with greater than proportional increases of plasma exposure with increasing dose both in humans and in rodents.[1,2] The possible causal factors for these phenomena include the glucuronidation of telmisartan and hepatobiliary transport of telmisartan and its acylglucuronide; however, further quantitative analyses are still needed to clarify their relative importance.

It has been reported that telmisartan is specifically taken up into hepatocytes by organic anion transporting polypeptide (OATP)1B3/*SLCO1B3*, and the biliary efflux of its glucuronide is thought to be mediated by multiple transporters such as multidrug resistance-associated protein 2 (MRP2)/*ABCC2*, multidrug resistance protein 1 (MDR1)/*ABCB1* and breast cancer resistance protein (BCRP)/*ABCG2*.[4−6] OATP1B3 is expressed on the sinusoidal membrane of hepatocytes and is thought to be involved in the transport of a wide variety of drugs together with OATP1B1.[7−9] Thus, the saturation of OATP1B3-mediated uptake at high doses was considered to be a possible mechanism for the nonlinear pharmacokinetics of telmisartan. The changes in OATP1B3-mediated transport activity caused by drug−drug interactions, genetic polymorphisms, or liver dysfunction sometimes affect the pharmacokinetics of OATP1B3 substrates, and subsequently their therapeutic

Received: March 31, 2011
Accepted: August 3, 2011
Revised: July 28, 2011
Published: August 03, 2011

efficacy and adverse effect. For example, Kiyotani et al. demonstrated that a genetic polymorphism of *SLCO1B3* (rs11045585), which encodes OATP1B3, increased the risk of docetaxel-induced neutropenia possibly due to the changes in plasma concentration of docetaxel.[10] Therefore, telmisartan may be applicable as a probe substrate for OATP1B3 in humans.

In general, pharmacokinetic analyses based on plasma concentration profiles in clinical studies provide information only on overall hepatic intrinsic clearance, but cannot separately evaluate the intrinsic transport activity of sinusoidal uptake and canalicular efflux. Recently, we proposed the concept of a rate-determining process governing overall hepatic elimination of anionic drugs.[11−14] We have demonstrated that the functional change of hepatic uptake and efflux transporters differently influence the plasma and tissue concentration of pravastatin by using physiologically-based pharmacokinetic model.[13] To directly validate our pharmacokinetic theory in vivo, methods for quantitative estimation of the time profile of tissue concentration of drugs in vivo are necessary for separately estimating the transport activity of hepatic uptake and efflux. Positron emission tomography (PET) is a powerful noninvasive method for molecular imaging in living systems. The high sensitivity and exceptional spatio−temporal resolution of PET make it a particularly useful tool for estimating the in vivo function of drug transporters in various tissues over time following intravenous administration of a radiolabeled drug. We have demonstrated the utility of PET for the evaluation of hepatobiliary transport using 15*R*-[^{11}C]TIC-Me, a potential ^{11}C-labeled PET probe for the functional analysis of Mrp2.[15] In order to evaluate hepatobiliary transport of telmisartan in vivo, we developed a new radiotracer, ^{11}C-labeled telmisartan for the functional analyses of Oatp transporters in hepatic uptake. The development of a quantitative PET imaging method using [^{11}C]telmisartan would enable the noninvasive kinetic assessment of hepatobiliary transport involving Oatp-mediated hepatic uptake in vivo, and may also demonstrate the feasibility of PET imaging with [^{11}C]telmisartan for the evaluation of hepatobiliary transport in humans, especially for the functional analysis of OATP1B3.

Here, we report PET imaging using [^{11}C]telmisartan to analyze its hepatobiliary transport in rats. This study allowed for simultaneous measurement of time profiles of the total radioactivities in the liver and bile in a single rat, resulting in the determination of the intrinsic uptake, canalicular efflux, and overall hepatic elimination of telmisartan. To gain an insight into the transporters responsible for hepatic uptake and canalicular efflux, kinetic parameters of [^{11}C]telmisartan elimination in rats treated with rifampicin, a potent Oatp inhibitor, were compared with those in control rats. In addition, PET study with [^{11}C]telmisartan was also performed with the coadministration of unlabeled telmisartan at various doses to investigate whether PET imaging analysis is applicable for evaluating the changes of hepatic uptake and biliary excretion with increased doses of telmisartan. Our approach will be a kind of pioneering study for the analysis of drug transporter function based on tissue concentration using noninvasive molecular imaging technology as well as radiometabolite analysis and blood pharmacokinetics.

MATERIALS AND METHODS

Materials. The precursor of [^{11}C]telmisartan was obtained by esterification of *N*-desmethyl telmisartan (BIBT9584) with trimethylsilyldiazomethane. BIBT9584 was kindly supplied from Boehringer Ingelheim Pharma KG (Biberach, Germany).

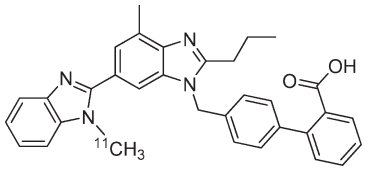

Figure 1. Chemical structures of [^{11}C]telmisartan.

^{11}C-Labeled telmisartan (Figure 1) was synthesized from BIBT9584 methyl ester by an N-methylation reaction with [^{11}C]methyl iodide, followed by ester hydrolysis. BIBT9584 methyl ester was reacted with [^{11}C]CH_3I in the presence of KOH in anhydrous DMSO at 80 °C for 5 min. 1 M NaOH was added to the mixture, and the resultant mixture was heated at 100 °C for 3 min, followed by treatment with acetic acid for 3 min at room temperature. Purification was performed by high-performance liquid chromatography (HPLC) on a COSMOSIL Cholester column (10 (i.d.) × 250 mm, 5 μm particle size) (Nacalai Tesque, Kyoto, Japan) using acetonitrile/10 mM ammonium acetate (55:45, pH 4.5) as the mobile phase. The purified fraction was concentrated and reconstituted with approximately 3 mL of saline containing 3% ethanol. The identity and concentration of [^{11}C]telmisartan were assessed by analytical HPLC. Radiochemical and chemical purity determined by UV absorbance at 254 nm was greater than 95%, and the specific radioactivity was 21−99 GBq/μmol at the time of injection. Rifampicin and unlabeled telmisartan were purchased from Sigma-Aldrich (St. Louis, MO). Rifampicin was dissolved in saline by adding an appropriate amount of 1 M NaOH. Unlabeled telmisartan was dissolved in 1 M NaOH, neutralized with 1 M HCl, and the solution was mixed with an equal volume of [^{11}C]telmisartan before administration. Each solution was prepared on the day of the experiments. All other organic solvents and reagents were of HPLC grade (Nacalai Tesque).

Animals. Male Sprague-Dawley (SD) rats weighing 220−290 g (7−8 weeks old, n = 3 for each set of experiments) were purchased from Japan SLC Inc. (Shizuoka, Japan). The animals were kept in a temperature- and light-controlled environment with standard food and tap water provided ad libitum. All experimental protocols were approved by the Ethics Committee on Animal Care and Use of the RIKEN Center for Molecular Imaging Science, and were performed in accordance with the Principles of Laboratory Animal Care (NIH publication No. 85-23, revised 1985).

PET Scans. All PET scans were performed using a microPET Focus220 scanner (Siemens, Knoxville, TN) designed for laboratory animals. This PET scanner has a spatial resolution of 1.4 mm in FWHM at the center of the view at 220 mm in diameter and an axial extent at 78 mm in length. PET experiments with [^{11}C]telmisartan, either alone, in combination with rifampicin, or with unlabeled telmisartan, were performed in male SD rats. Rats were anesthetized and maintained with a mixture of 1.5% isoflurane and nitrous oxide/oxygen (7:3), and the femoral artery was cannulated with polyethylene tubing for collection of blood samples. Before emission scanning, animals were placed in the center of the PET camera, and a 25 min transmission scan with a rotating ^{68}Ge−^{68}Ga point source was performed for the abdomen positioning and attenuation correction. At the start of the emission scan, [^{11}C]telmisartan was administered as a single bolus via the tail vein in doses of 57−134 MBq/kg. The chemical amount of [^{11}C]telmisartan for the bolus injection was calculated as 0.20−1.4 nmol/body (0.10−0.72 μg/body).

For the functional analysis of Oatp in hepatic uptake, rifampicin, a typical Oatp inhibitor, was intravenously infused at a rate of 0.5 or 1.5 μmol/min/kg for at least 90 min before the administration of [^{11}C]telmisartan, and then a constant infusion was kept until the end of the PET scan. In addition, PET studies with [^{11}C]telmisartan coinjected with unlabeled telmisartan (1, 4, and 10 mg/kg) was performed to investigate the changes in hepatobiliary transport including the saturation of hepatic uptake with increasing doses of unlabeled telmisartan.

An emission scan in 3D list-mode was performed for 90 min and sorted into 75 dynamic sinograms according to the following sequence: 24 × 5 s, 26 × 30 s, 25 × 180 s. Arterial blood was sampled via the cannulated femoral artery 13 times within 90 min at the following time points: 10, 20, 30, 40, and 50 s and 1, 2, 5, 10, 20, 40, 60, and 90 min after administration of [^{11}C]telmisartan. The volume of blood sampled for each time point was within 120 μL, and the total blood volume sampled from one rat did not exceed 1.6 mL, about 10% of total circulating blood volume. Blood radioactivity was measured using a 1470 WIZARD automatic gamma counter (PerkinElmer, Waltham, MA, USA). The radioactivity in each measured sample was corrected for time decay from the point of [^{11}C]telmisartan. After finishing the PET scan, anesthesia was maintained at 1.5% isoflurane before euthanasia by exsanguination via aortic puncture.

Analysis of PET Imaging Data. PET images were reconstructed using microPET manager 2.4.1.1 (Siemens) by Fourier Rebinning (FORE) and standard 2D filtered back projection (FBP) using a ramp filter with a cutoff at the Nyquist frequency, or by FORE and maximum likelihood expectation maximization (MLEM). Compared with FBP, MLEM reconstruction of small animal PET images provides better spatial resolution and statistical noise properties, which is advantageous for the delineation of regions of interest (ROIs). On the other hand, FBP reconstructed images were used for quantification because FBP is superior to the other reconstruction method in quantification. Regions of interest (ROIs) representing the liver and the intestines were delineated using the Pmod ver. 3.0 program (PMOD Technologies Ltd., Zurich, Switzerland) as follows. First, ROIs were defined on tissue images derived from the summation of appropriate time frames after [^{11}C]-telmisartan administration, in which these tissues could easily be identified. Especially, liver and intestine showed the uptake of significant radioactivity; therefore it is easier to identify relative anatomic locations and the shape of the liver and also some parts of the intestine in summated PET images. The position of the liver was also confirmed by CT anatomical images in another animal with the same posture, the empirical anatomic information in rats and the use of the information of the rat body surface in the same animal, identified by transmission scan conducted before the [^{11}C]telmisartan PET. 3D-VOI definitions of liver and intestine were then used to visually inspect for possible movement artifacts between sequential scans in the same segment. All ROIs were combined and changed to volumetric regions of interest (VOIs).

For the liver images, the scaling of the images was determined so that the distribution of [^{11}C]telmisartan in the liver appeared very intense but enough contrast was present to distinguish clearly liver structures in the summated PET images for the initial few minutes after [^{11}C]telmisartan administration. The VOIs of the liver were optimized by fitting the images to show the similar degree of liver weight in the individual animal. For the images of intestine, it is more difficult to distinguish the whole shape of the intestine, but easier to define the hot area in the intestine in each sequential scan. As the total radioactivity amount in the tissue is necessary for the analysis of intestinal radioactivity, the VOIs were constructed on the PET images to include all intestinal activity in the sequential scans but not to include stomach, liver, kidney, and spleen. In this PET analysis, the radioactivity in the intestine corresponds to that in bile excreted to the intestine. Thus the radioactivity in the intestine was described in this study as "the radioactivity in intestine (the radioactivity in bile excretion into intestine)". Time−radioactivity curves for each tissue were constructed by normalizing decay-corrected time−radioactivity measurements to the injected dose (% dose) of [^{11}C]telmisartan.

Kinetic Analysis. Initial [^{11}C]telmisartan uptake rate in rat liver was calculated by the integration plot method[16] using the portion of time profile of the radioactivity encompassing about the first 2 min after [^{11}C]telmisartan administration, during which biliary excretion from the liver and metabolism were negligible. The hepatic uptake clearance of [^{11}C]telmisartan was determined using eq 1:

$$\frac{X_{t,\mathrm{liver}}}{C_{t,\mathrm{blood}}} = \mathrm{CL}_{\mathrm{uptake,liver}} \times \frac{\mathrm{AUC}_{0-t,\mathrm{blood}}}{C_{t,\mathrm{blood}}} + V_{\mathrm{E}} \quad (1)$$

where $X_{t,\mathrm{liver}}$ is the amount of ^{11}C radioactivity in the liver at time t as determined by PET image analysis. $C_{t,\mathrm{blood}}$ is the concentration of [^{11}C]telmisartan in blood at time t, as determined by the measurement of radioactivity in blood taken from the femoral artery with gamma counter. $\mathrm{CL}_{\mathrm{uptake,liver}}$ is the uptake clearance in the liver, and $\mathrm{AUC}_{0-t,\mathrm{blood}}$ is the area under the blood concentration−time curve from time 0 to time t. The $\mathrm{CL}_{\mathrm{uptake,liver}}$ value can be obtained from the initial slope of the plots of $X_{t,\mathrm{liver}}/C_{t,\mathrm{blood}}$ versus $\mathrm{AUC}_{0-t,\mathrm{blood}}/C_{t,\mathrm{blood}}$. V_{E} represents the initial distribution volume in the liver at time 0, calculated from the y-intercept of the integration plot.

Biliary excretion clearance was estimated by integration plot analysis using noninvasive measurements of radioactivity in the liver and the intestine (the radioactivity in bile excreted into the intestine) between 5 and 40 min after drug administration. The biliary excretion clearance of the radioactivities is described by the following equation:

$$X_{t,\mathrm{bile}} = \mathrm{CL}_{\mathrm{int,bile}} \times \mathrm{AUC}_{0-t,\mathrm{liver}} + X_{\mathrm{E}} \quad (2)$$

where $X_{t,\mathrm{bile}}$ is the amount of ^{11}C radioactivity in the intestine (the radioactivity in bile excreted into the intestine) at time t, as determined by PET image analysis. $\mathrm{CL}_{\mathrm{int,bile}}$ represents the intrinsic biliary clearance of [^{11}C]telmisartan-associated radioactivity in the liver, and $\mathrm{AUC}_{0-t,\mathrm{liver}}$ is the area under the hepatic concentration−time curve from time 0 to time t. The $\mathrm{CL}_{\mathrm{int,bile}}$ value can be obtained from the slope of the plots of $X_{t,\mathrm{bile}}$ versus $\mathrm{AUC}_{0-t,\mathrm{liver}}$. X_{E} was calculated as the y-intercept of the integration plot.

Radiometabolite Analysis of Rat Blood, Liver, and Bile Using Radiometric HPLC. Radiometabolite analysis of rat blood, liver, and bile was performed separately from the PET study to evaluate the average values of time profiles of the metabolite composition in the tissue. Venous blood samples were collected at 20 min after administration of [^{11}C]telmisartan. To sample bile, the bile duct in SD rats was cannulated before [^{11}C]telmisartan administration, and bile was collected over the periods of 0−10, 10−20, and 20−40 min after administration (the sampling volume: 141 ± 46 μL/10 min). After sampling the blood or bile, anesthesia was maintained at 1.5% isoflurane before euthanasia by exsanguination via aortic puncture. To sample liver tissue, blood flow was terminated by exsanguination via abdominal aortic puncture at 5, 20, and 40 min postadministration, and the liver was quickly removed and homogenized. Blood, bile, and liver homogenates

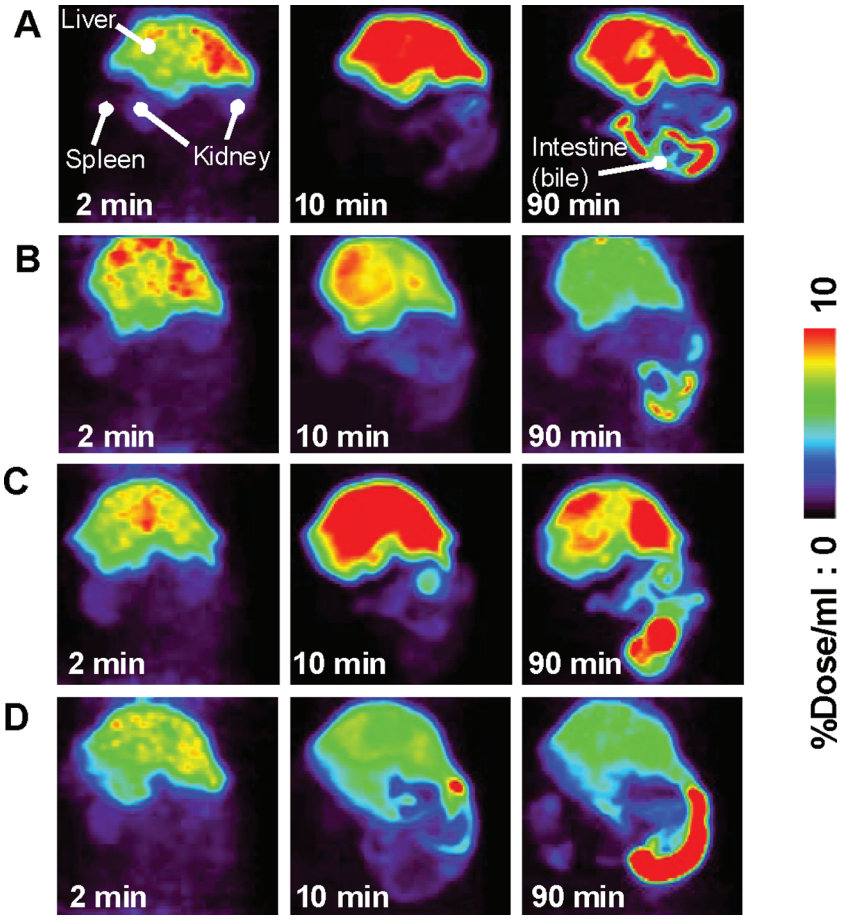

Figure 2. Color-coded PET images of rat abdominal regions taken after intravenous administration of [^{11}C]telmisartan. Colonal maximum intensity projecting PET images of radioactivity in the abdominal region were captured at 2, 10, and 90 min in control rats (A), rifampicin-treated rats at an infusion rate of 1.5 μmol/min/kg (B), and rats treated with unlabeled telmisartan at a dose of 1 mg/kg (C) and 10 mg/kg (D).

were deproteinated by precipitation with acetonitrile. After centrifugation, the supernatants were evaporated, reconstituted with HPLC mobile phase and then analyzed for radioactive components using an HPLC system (Shimadzu Corporation, Kyoto, Japan) with a coupled NaI(TI) positron detector UG-SCA30 (Universal Giken, Kanagawa, Japan) to measure the intact radiotracer and its metabolites. The lower limit of the detection of the detector is 100 Bq/injection, which is sufficient for the metabolite analysis of the tissue samples taken by 40 min postadministration. Chromatographic separation was carried out using a Waters Atlantis T3 column (4.6 (i.d.) × 50 mm; Waters, Milford, MA). The flow was 2.0 mL/min at initial conditions of 70% solvent A (10% acetonitrile in 2 mM ammonium formate including 0.1% formic acid (pH 3)), and 30% solvent B (80% acetonitrile in 2 mM ammonium formate including 0.1% formic acid (pH 3)). Analytes were eluted using the following gradient conditions: 0 to 0.5 min, 30% solvent B in solvent A; 0.5 to 2.5 min, 10% to 100% solvent B in solvent A; 2.5 to 4 min, 100% solvent B. Following the elution, the column was returned to 30% solvent B in solvent A over 2 min. The elution was monitored by UV absorbance at 300 nm and coupled NaI positron detection. The individual peak areas of the radiometric HPLC chromatograms were corrected for radioactive decay to the retention time of radiometabolite for each sample and expressed as fractions of total radioactivity. The previously determined total radioactivity concentrations (expressed as percentage of the injected dose) in the liver and bile were multiplied by the decay corrected fraction of unmetabolized [^{11}C]telmisartan or radiometabolites ([^{11}C]telmisartan-acylglucuronide) to generate metabolite corrected time−radioactivity profiles in liver or bile. The amount of radioactivity associated with intact [^{11}C]telmisartan and its metabolites was calculated as the percentage of the total amount of radioactivity.

Statistical Analysis. Data were calculated as the mean ± SD for three determinations. A Student's two-tailed unpaired *t*-test was used to identify significant differences between groups. Statistical significance was set at $p < 0.05$.

RESULTS

Distribution of the Radioactivity in the Abdominal Region of Rats Following Iv Administration of [^{11}C]Telmisartan. The maximum intensity projection PET images of radioactivity in the abdominal region over time following administration of [^{11}C]-telmisartan to control rats or rats treated with rifampicin or unlabeled telmisartan are shown in Figure 2. Radioactivity was localized primarily in the liver in all kinds of animals by 2 min postadministration, and subsequently part of the radioactivity moved to the intestine. The radioactivity detected in the intestine corresponds to the excretion of [^{11}C]telmisartan and/or its metabolites into the bile, which was consistent with the radioactivity in bile sampled from bile duct cannulated rats (data not

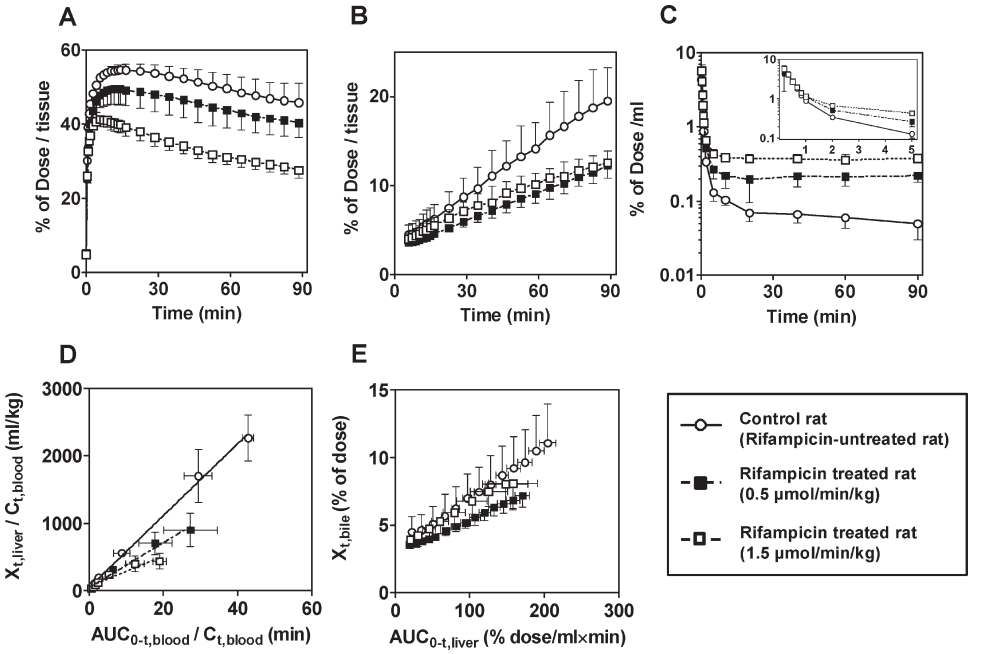

Figure 3. Time profiles of the radioactivity in tissues and blood, and integration plots for the determination of hepatic uptake and biliary efflux in control rats and rifampicin-treated rats after intravenous administration of [^{11}C]telmisartan. The time profiles of the radioactivity in the liver (A), intestine (the radioactivity in bile excreted into the intestine) (B), and blood (C) were determined using PET imaging and blood sampling over a 90 min period following iv administration of [^{11}C]telmisartan. The inset of (C) shows the detailed curves in the early time period of blood radioactivity. Integration plots were drawn for the calculation of hepatic uptake (D) and biliary efflux (E) of total radioactivity in control rats and rifampicin-treated rats. The data represent the mean ± SD (n = 3).

shown). Other organs that showed radioactivity above the background level included the spleen and kidney. The radioactivity in the spleen and kidney was detected just after postadministration, but it was markedly decreased to the background level even at 10 min.

Compared to the distribution of the radioactivity in control rats (Figure 2A), the radioactivity in the liver and the intestine was lower in rats treated with the constant infusion of 1.5 μmol/min/kg rifampicin (Figure 2B). The radioactivity in the abdominal region of rats coadministered with 1 mg/kg unlabeled telmisartan (Figure 2C) was similar to that in rats treated only with radiotracer. In contrast, a decrease in radioactivity in the liver and an increase in the intestine were observed in rats coadministered with 10 mg/kg unlabeled telmisartan (Figure 2D) compared to the images in rats only with radiotracer.

Tissue Distribution, Metabolism, and Hepatobiliary Transport of the Radioactivity Following Iv Administration of [^{11}C]Telmisartan in Rats. Time profiles of the radioactivity in tissues in the abdominal regions and blood are shown in Figures 3A−3C. In control rats, a maximum of 55 ± 1% of the dose was distributed in the liver at 14 min of postadministration and the radioactivity began to fall gradually until 90 min, the end of the PET scan (Figure 3A). The radioactivity in the intestine, which corresponds to the radioactivity in the bile excreted into the intestine, gradually increased until 90 min, and reached 20 ± 4% of the dose at 90 min of postadministration (Figure 3B). The radioactivity in the blood was rapidly decreased within 5 min, and then slightly decreased until 90 min in control rats (Figure 3C). These results showed that [^{11}C]telmisartan-associated radioactivity was primarily excreted via hepatobiliary transport in rats.

Figure 4A shows representative radiochromatograms of extracts from blood, liver, and bile prepared 20 min after administration of [^{11}C]telmisartan to rats. Radiometric HPLC analyses revealed that almost 100% of the radioactivity in the blood at 20 min and more than 94% of the radioactivity in the liver was present as a parent compound at 5, 20, and 40 min postadministration. On the other hand, most of the radioactivity excreted into bile collected over the periods of 0−10, 10−20, 20−40 min after administration of [^{11}C]-telmisartan was derived from the radiometabolite of [^{11}C]telmisartan. As we confirmed that the retention time of the major radiometabolite was equivalent to that of telmisartan-acylglucuronide, the radiometabolite detected in this PET study is considered to be [^{11}C]telmisartan-acylglucuronide. These results were consistent with the previous reports that unlabeled telmisartan was extensively metabolized in the liver by conjugation with glucuronic acid in humans as well as rats, and then the major metabolite, telmisartan acylglucuronide, was excreted into bile.[17] Time profiles of the radioactivity of [^{11}C]telmisartan and its radiometabolites in the liver and the intestine (the radioactivity in bile excreted into the intestine) are shown in Figures 4B and 4C, which was calculated by the products of time profiles of the [^{11}C]telmisartan-associated radioactivity and the composition of [^{11}C]telmisartan or its radiometabolite in the tissues at 5, 20 and 40 min postadministration.

The pharmacokinetic parameters estimated from integration plots are shown in Table 1. The integration plots were linear in the liver for a short period, which varied from 0.3 to 2.0 min after the administration of [^{11}C]telmisartan (Figure 3D). During this period, the ^{11}C radioactivity in the blood and the liver was derived primarily from [^{11}C]telmisartan, and the amount of [^{11}C]telmisartan-acylglucuronide was negligible considering the results of the radiometric HPLC analysis in blood at 20 min and liver at 5 min postadministration. The hepatic uptake clearance ($CL_{uptake,liver}$) in control rats was calculated to be 63 ± 11 mL/min/kg (Table 1), which is very close to the hepatic blood flow rate in rats.[18] In addition, the integration plots for the calculation of biliary efflux clearance of radioactivity are shown in Figure 3E, in which $AUC_{0-t,liver}$ and $X_{t,bile}$ (the radioactivity in bile excreted into the intestine) were estimated by the noninvasive

dx.doi.org/10.1021/mp200160t |*Mol. Pharmaceutics* 2011, 8, 1789–1798

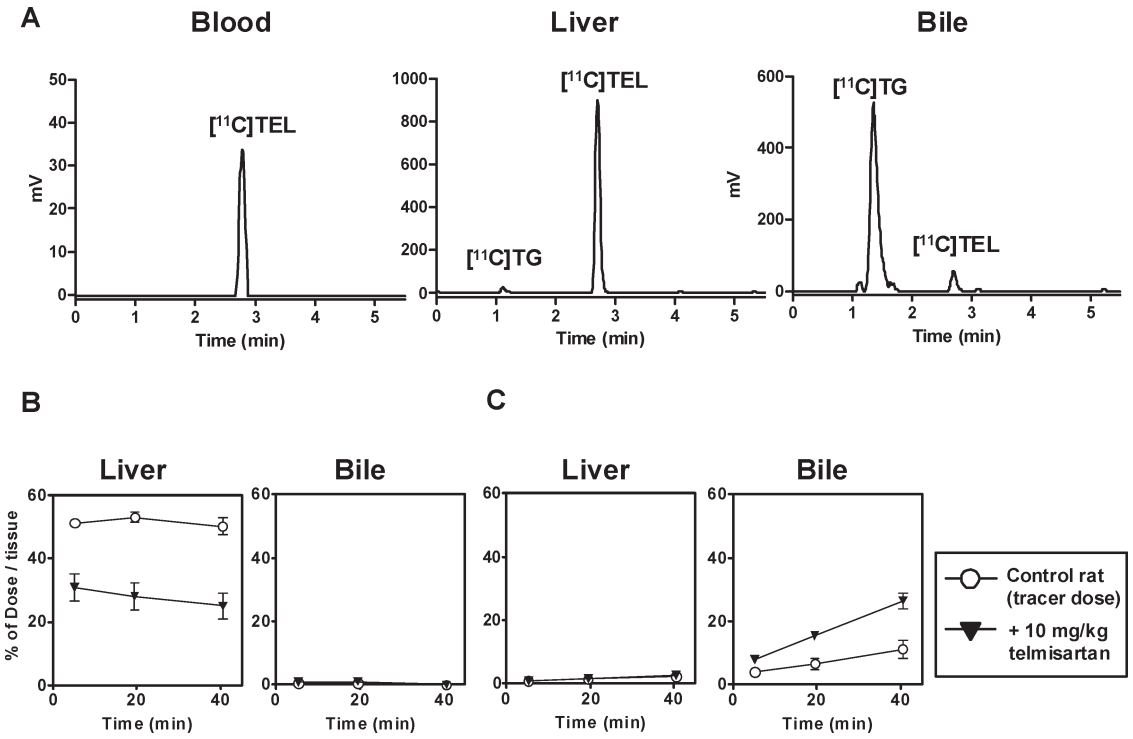

Figure 4. Representative HPLC radiochromatograms of blood, liver, and bile extracts and time profiles of the radioactivity in the liver and bile for [^{11}C]telmisartan and [^{11}C]telmisartan acylglucuronide in rats following intravenous administration of [^{11}C]telmisartan. HPLC radiochromatograms of blood extracts at 20 min, liver extracts at 20 min and bile from 10−20 min following administration of [^{11}C]telmisartan (A). The individual peak areas of the radiometric HPLC chromatograms were corrected for radioactive decay to the retention time of radiometabolite for each sample and expressed as fractions of total radioactivity. The previously determined total radioactivity concentrations (expressed as percentage of the injected dose) in the liver and bile were multiplied by the decay corrected fraction of unmetabolized [^{11}C]telmisartan or radiometabolites ([^{11}C]telmisartan-acylglucuronide) to generate metabolite corrected time−radioactivity profiles in the liver at 5, 20, and 40 min and in the bile collected over the periods of 0−10, 10−20, 20−40 min after administration of [^{11}C]telmisartan. Time profiles of the radioactivity for [^{11}C]telmisartan (B) and [^{11}C]telmisartan-acylglucuronide (C) in the liver and bile, which corresponds to the radioactivity in bile excreted into the intestine, are plotted for control rats and rats coadministered with unlabeled telmisartan at a dose of 10 mg/kg. Data represent the mean ± SD (n = 3). [^{11}C]TEL: [^{11}C]telmisartan. [^{11}C]TG: [^{11}C]telmisartan-acylglucuronide.

Table 1. Pharmacokinetic Parameters of [^{11}C]Telmisartan after Its Intravenous Administration in Rats[a]

		+ rifampicin (infusion rate, μmol/min/kg)		+ unlabeled telmisartan (mg/kg)		
	control (tracer dose)	0.5	1.5	1	4	10
$AUC_{0-90min,blood}$ (% dose × min/mL)	9.5 ± 1.9	23 ± 5*	37 ± 5***	12 ± 1	28 ± 7*	42 ± 11**
$CL_{uptake,liver}$ (mL/min/kg)	63 ± 11	46 ± 6	41 ± 3*	46 ± 13	36 ± 8	33 ± 3**
V_E (ml/kg)	9.7 ± 5.9	9.3 ± 3.1	14 ± 1	8.8 ± 3.6	6.2 ± 0.9	13 ± 4
$CL_{int,bile,RA}$ (mL/min/kg)	0.15 ± 0.04	0.10 ± 0.03	0.13 ± 0.02	0.17 ± 0.02	0.50 ± 0.13*	0.67 ± 0.15**
$CL_{int,bile,TG}$ (mL/min/kg)	5.7 ± 1.5	ND	ND	ND	ND	11 ± 2*

[a] $CL_{uptake,liver}$ and V_E were obtained by integration plot analyses with eq 1. $CL_{int,bile,RA}$ and $CL_{int,bile,TG}$ were obtained by integration plot analyses with eq 2. The values represent the mean ± SD (n = 3). A statistically significant difference was observed compared to control rats (t-test, * $p < 0.05$, ** $p < 0.01$, *** $p < 0.001$). ND: not determined.

measurement of radioactivity with PET image analysis. The intrinsic biliary efflux clearance ($CL_{int,bile}$) in control rats was 0.15 ± 0.04 mL/min/kg (Table 1).

The Effect of Rifampicin Coadministration on the Hepatobiliary Transport of [^{11}C]Telmisartan. Time profiles of the radioactivity in tissues and blood in rifampicin-treated rats are shown in Figures 3A−3C. The radioactivity in the liver was decreased in rifampicin-treated groups in a dose-dependent manner of rifampicin (Figure 3A), whereas the radioactivity in the intestine (the radioactivity in bile excreted into the intestine) was slightly decreased in rifampicin-treated groups (Figure 3B). In addition, the blood radioactivity was significantly increased in rifampicin-treated rats and the $AUC_{0-90min}$ of the blood was 2.4-fold and 3.9-fold higher in rats treated with constant infusion of rifampicin at a rate of 0.5 and 1.5 μmol/min/kg, respectively, than that in control rats (Figure 3C). Kinetic analyses showed that hepatic uptake clearance ($CL_{uptake,liver}$) of [^{11}C]telmisartan was significantly decreased to 41 ± 3 mL/min/kg in the rats treated with constant infusion of 1.5 μmol/min/kg rifampicin (Table 1). On the other hand, V_E values of [^{11}C]telmisartan were not significantly different among control rats and rats treated with low and high doses of rifampicin and they were comparable to the vascular space in the

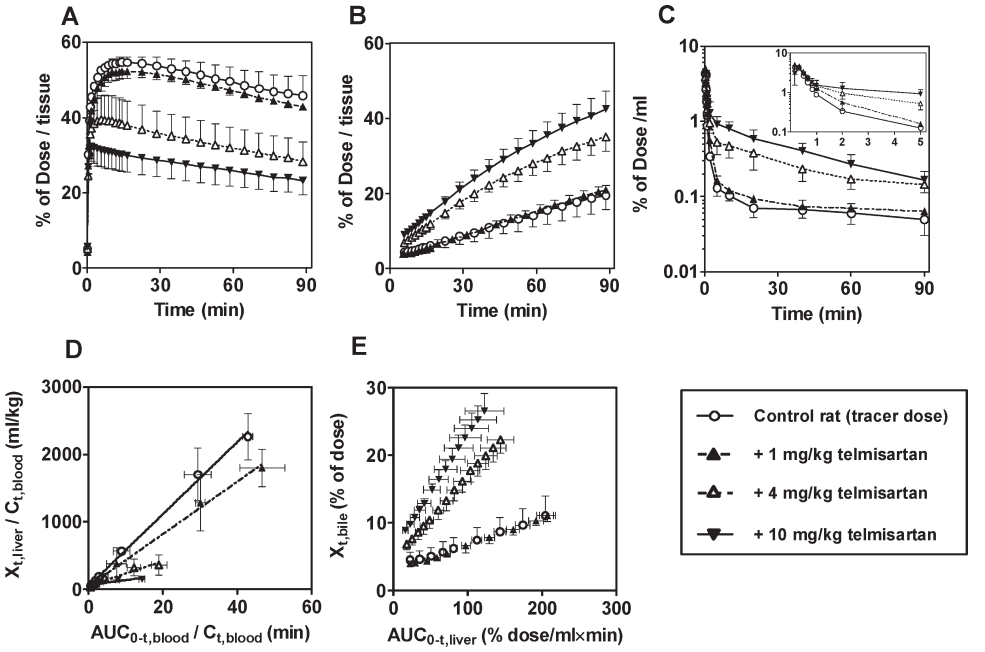

Figure 5. Time profiles of the radioactivity in tissues and blood, and integration plots for the determination of hepatic uptake and biliary efflux in control rats (tracer dose) and rats coadministered with unlabeled telmisartan after intravenous administration of [^{11}C]telmisartan. The time profiles of the radioactivity in the liver (A), intestine (the radioactivity in bile excreted into the intestine) (B), and blood (C) were determined using PET imaging and blood sampling over a 90 min period following iv administration of [^{11}C]telmisartan. The inset of (C) shows the detailed curves in the early time period of blood radioactivity. Integration plots were drawn for the calculation of hepatic uptake of [^{11}C]telmisartan in control rats and rats in combination with unlabeled telmisartan (D). Integration plots were drawn for the calculation of hepatic uptake (D) and biliary efflux (E) of total radioactivity in control rats and rats coadministered with unlabeled telmisartan. The data represent the mean ± SD (n = 3).

liver.[19] In addition, there was no significant difference in the biliary efflux clearance ($CL_{int,bile}$) of ^{11}C-radioactivity between control rats (0.15 ± 0.04 mL/min/kg) and rifampicin-treated rats (0.10 ± 0.03 mL/min/kg and 0.13 ± 0.02 mL/min/kg at an infusion rate of 0.5 and 1.5 μmol/min/kg, respectively) (Table 1).

The Effect of Various Doses of Unlabeled Telmisartan on the Hepatobiliary Transport of [^{11}C]Telmisartan. Time profiles of the radioactivity in tissues and blood in rats following administration of [^{11}C]telmisartan at a tracer dose (about 3 μg/kg) or coadministration of the radiotracer with 1, 4, and 10 mg/kg of unlabeled telmisartan are shown in Figures 5A−5C. At a dose of 1 mg/kg telmisartan, the time profiles of the radioactivity in the liver, intestine (the radioactivity in bile excreted into the intestine) and blood were almost similar to those at a tracer dose, and the $CL_{uptake,liver}$ was 46 ± 13 mL/min/kg, which was decreased by 27% compare to that at a tracer dose, though it did not reach a statistically significant difference. At a dose of 4 and 10 mg/kg telmisartan, the radioactivity in the liver was decreased and the blood radioactivity was increased, which results in the significant decrease in the $CL_{uptake,liver}$ to 36 ± 8 and 33 ± 3 mL/min/kg, respectively, compared to that at a tracer dose (Figures 5A and 5C and Table 1). On the other hand, the radioactivity in the intestine (the radioactivity in bile excreted into the intestine) was significantly increased at a dose of 4 or 10 mg/kg telmisartan (Figure 5B). The $CL_{int,bile}$ of ^{11}C-radioactivity at a dose of 1, 4, and 10 mg/kg telmisartan was 0.17 ± 0.22, 0.50 ± 0.13, and 0.67 ± 0.15 mL/min/kg, respectively (Table 1). The biliary excretion of ^{11}C-radioactivity was increased by increasing the unlabeled telmisartan dose. As the metabolite analysis revealed that the majority of the radioactivity in the liver was present as a parent compound, and the radioactivity excreted into bile existed as [^{11}C]telmisartan-acylglucuronide (Figure 4A), the

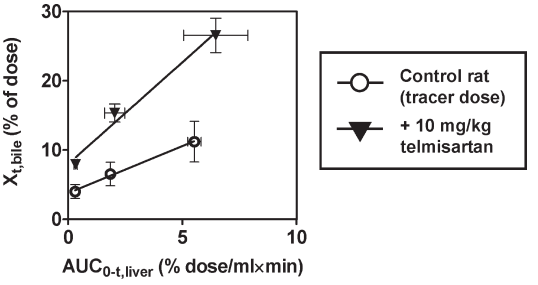

Figure 6. Integration plots for the biliary efflux of [^{11}C]telmisartan-acylglucuronide after intravenous administration of [^{11}C]telmisartan in rats with or without coadministration of unlabeled telmisartan. Integration plots were drawn for the determination of the biliary efflux of [^{11}C]telmisartan-acylglucuronide in control rats and rats coadministered with unlabeled telmisartan at a dose of 10 mg/kg. The previously determined total radioactivity concentrations in the liver and bile were multiplied by the decay corrected fraction of unmetabolized [^{11}C]telmisartan or radiometabolites ([^{11}C]telmisartan-acylglucuronide) in control rat or rats coadministered with unlabeled telmisartan to generate metabolite corrected time−radioactivity profiles in the liver at 5, 20, and 40 min and in the bile collected over the periods of 0−10, 10−20, and 20−40 min after administration of [^{11}C]telmisartan, and then $AUC_{0-t,liver}$ and $X_{t,bile}$ of [^{11}C]telmisartan-acylglucuronide were determined. The data represent the mean ± SD (n = 3).

intrinsic clearance for the biliary excretion of [^{11}C]telmisartan-acylglucuronide ($CL_{int,bile,TG}$) was estimated from integration plot analysis by using the time profile of the radioactivity for [^{11}C]-telmisartan-acylglucuronide in the liver and intestine (the radioactivity in bile excreted into the intestine) (Figure 6). There were still large differences in $CL_{int,bile,TG}$ value between a tracer dose and

dx.doi.org/10.1021/mp200160t |*Mol. Pharmaceutics* 2011, 8, 1789–1798

a dose of 10 mg/kg telmisartan (5.7 ± 1.5 and 11 ± 2 mL/min/kg, respectively) (Table 1).

DISCUSSION

In the present study, kinetic analyses of hepatobiliary transport of [^{11}C]telmisartan were carried out in rats to demonstrate that PET imaging enables simultaneous determination of the changes in hepatic sinusoidal uptake and canalicular efflux, separately in a single animal. The purpose of this PET study using [^{11}C]telmisartan was to quantitatively evaluate the hepatobiliary transport of telmisartan mediated by transporters in rats and its change by the coadministration of various doses of rifampicin or unlabeled telmisartan. Our results show that the hepatic uptake of [^{11}C]telmisartan was significantly decreased in rats treated with rifampicin, a potent Oatp inhibitor, and unlabeled telmisartan. In addition, the biliary excretion of the radioactivity was increased when increasing the dose of unlabeled telmisartan, whereas there was no significant change of the parent/radiometabolite fraction in the liver and biles. These results suggest that PET imaging with [^{11}C]telmisartan is applicable at least to the characterization of the hepatic uptake mediated by Oatp transporters in vivo.

After intravenous administration, [^{11}C]telmisartan was primarily distributed in the liver, extensively metabolized to [^{11}C]telmisartan acylglucuronide, and the metabolite-associated radioactivity was excreted into the bile in control rats. The uptake of telmisartan into rat hepatocytes was reported to be inhibited by several Oatp inhibitors including digoxin (a specific inhibitor for Oatp1a4),[5] indicating that the hepatic uptake of [^{11}C]telmisartan in rats was mainly mediated by Oatps including Oatp1a4. In order to evaluate the potential effect of Oatp inhibition on the hepatic uptake of [^{11}C]telmisartan, we chose to use rifampicin as a potent inhibitor of Oatps. Rifampicin is a well-known inducer of CYP enzymes,[20] P-glycoprotein and MRP2 upon multiple dosing,[21,22] but rifampicin is also a potent inhibitor of OATP1B1 and OATP1B3 even following only a single dose.[8,23] The present PET image analyses showed that rifampicin inhibited the hepatic uptake of [^{11}C]telmisartan in rats. As $CL_{uptake,liver}$ of [^{11}C]telmisartan was almost the same as hepatic blood flow rate in control rats, it was difficult to accurately calculate the intrinsic hepatic uptake clearance (PS_{inf}) in rats. On the other hand, coadministration of rifampicin significantly decreased the $CL_{uptake,liver}$ of [^{11}C]telmisartan, suggesting the drastic decrease in the PS_{inf} mediated by Oatps in rats. Although we cannot quantitatively calculate the decrease in the PS_{inf} values, we can discuss whether rifampicin could inhibit the Oatp-mediated transport of [^{11}C]telmisartan in this study by comparing the K_i values of rifampicin for Oatp transporters and protein unbound plasma concentration of rifampicin. Rifampicin concentration in the plasma at an infusion rate of 1.5 μmol/min/kg was 101−118 μM during the PET scan, which is determined by LC/MS/MS analysis. Considering the protein unbound fraction of rifampicin in the plasma (0.1−0.4),[24] the plasma unbound concentration of rifampicin was calculated to be 10−47 μM, which is larger than the K_i values for OATP1B3 (~5 μM) in human, and Oatp1a1 (18.2 μM) Oatp1a4 (1.4−2.9 μM) and Oatp1b2 (0.79 μM) in rats.[8,25−27] Thus, the increase of plasma concentration of [^{11}C]telmisartan can be reasonably explained by the inhibition of Oatp transporters by rifampicin. In the previous report of human clinical study, a single dose of rifampicin, whose maximum plasma concentration is about 8 μM, increased the plasma concentration of atorvastatin, a substrate of OATPs.[8] This result is also in good agreement with a previous report using ex situ isolated perfused rat liver demonstrating the inhibition of Oatp-mediated hepatic uptake of atorvastatin by coadministration of rifampicin.[26]

We also performed a PET study with [^{11}C]telmisartan in coadministration with various doses of unlabeled telmisartan to demonstrate whether PET imaging analysis is applicable for estimating the changes in hepatic uptake and the biliary efflux when increasing the dose of telmisartan. Coadministration of unlabeled telmisartan at a dose of more than 4 mg/kg resulted in the decrease of hepatic sinusoidal uptake clearance as well as the increase of canalicular efflux clearance. On the other hand, the change of the parent/metabolite ratio was not significantly changed even at a dose of 10 mg/kg telmisartan compared to that at a tracer dose. The lack of significant change in the metabolism of [^{11}C]telmisartan in this rat study may have been caused by the different route of administration (iv injection), since the contribution of glucuronidation in the intestine is to be underestimated compared to the case of the oral administration. The in vitro study showed that the in vitro K_m value for telmisartan uptake into rat hepatocytes was 21.7 ± 4.4 μM in the presence of 1% human serum albumin (HSA), and the apparent K_m value of telmisartan in rat plasma was estimated to be 115 μM by using the protein unbound fraction of telmisartan in 1% HSA and rat plasma.[5] The initial blood concentration of telmisartan after intravenous administration of 10 mg/kg dose was 65−217 μM, which was comparable to the apparent K_m values, showing enough exposure of telmisartan in the blood for the self-saturation of hepatic uptake at this dose.

It has been reported that the rate-limiting process of the hepatic elimination is variable across the species in some drugs such as methotrexate because of the difference in their transport activities in both sinusoidal and canalicular efflux.[11,28,29] Plasma clearance of telmisartan in humans has been calculated to be 7.7 mL/min/kg,[1,2] which is less than the half of the hepatic blood flow rate, whereas in vivo $CL_{uptake,liver}$ of [^{11}C]telmisartan in rats is very close to the hepatic blood flow rate. In addition, Ishiguro et al. showed that uptake clearance of telmisartan was calculated to be 15 μL/min/10^6 cells into rat hepatocytes in the presence of 1% HSA (927 μL/min/10^6 cells in the absence of HSA) and 17−49 μL/min/10^6 cells in human hepatocytes in the presence of 0.3% HSA (304−875 μL/min/10^6 cells in the absence of HSA), showing that intrinsic uptake clearance into human hepatocytes was relatively lower than that into rat hepatocytes.[5] Thus, we expected that kinetic assessment of the hepatic uptake of telmisartan can be performed more quantitatively in humans by PET image analyses with [^{11}C]telmisartan because we can accurately estimate the PS_{inf} values in humans.

Regarding the change in the biliary efflux of radioactivity with increased doses of unlabeled telmisartan, we have no clear answer. $CL_{int,bile}$ is calculated as the product of PS_{bile} (intrinsic clearance of canalicular efflux from hepatocytes to bile) and f_H (protein unbound fraction in the liver tissue). Thus one of the possible mechanisms is the saturation of protein binding in the liver, resulting in an increase of f_H values of telmisartan-acylglucuronide. The saturation of protein binding of telmisartan-acylglucuronide in the liver should be conducted in the future.

Studies using imaging technologies, such as PET, single-photon emission computed tomography (SPECT), and magnetic resonance imaging (MRI), provide information on drug transport into and out of tissues based on the tissue concentration and thus contribute to the improvement of the predictability/reliability of in vitro to in vivo extrapolation of drug transport. Some probes for these imaging technologies are substrates of OATPs such as gadolinium-ethoxybenzyl-diethylenetriamine pentaacetic acid (Gd-EOB-DTPA),

which is a magnetic resonance imaging contrast agent and a substrate of OATP1B1, OATP1B3 and NTCP,[30] and ^{99m}Tc-mebrofenin, a substrate of OATP1B1, OATP1B3, MRP2 and MRP3.[31,32] However, no reports so far have functionally analyzed OATP1B3 exclusively. The present study functionally analyzed Oatps in rats using PET imaging with [^{11}C]telmisartan, a specific substrate of OATP1B3, and demonstrated the feasibility of PET imaging with [^{11}C]telmisartan for simultaneous determination of separate changes in hepatic sinusoidal uptake and canalicular efflux in humans, especially for functional analysis of OATP1B3.

In conclusion, we demonstrated the high potential of noninvasive PET imaging to investigate the hepatobiliary transport of [^{11}C]-telmisartan by separate quantitative evaluation of hepatic uptake and biliary efflux in rats. The usefulness of [^{11}C]telmisartan was also demonstrated for functional analysis of Oatps in hepatic uptake in rats and for understanding the saturable uptake process of telmisartan. The guidance of microdose clinical study has been released recently in which the use of PET is recommended to determine the tissue distribution of compounds in humans.[33] The present study with [^{11}C]telmisartan is expected to provide the feasibility of PET imaging study to investigate the transport function of OATP1B3 in humans.

AUTHOR INFORMATION

Corresponding Author

*Molecular Probe Dynamics Laboratory, RIKEN Center for Molecular Imaging Science, 6-7-3 Minatojima-minamimachi, Chuo-ku, Kobe, Hyogo 650-0047, Japan. Phone: +81-78-304-7124. Fax: +81-78-304-7126. E-mail: ttakashima@riken.jp.

ACKNOWLEDGMENT

This study is a part of the Research Project for the "Establishment of Evolutional Drug Development with the Use of Microdose Clinical Trial" sponsored by the New Energy and Industrial Technology Development Organization (NEDO). We are indebted to Masahiro Kurahashi of Sumitomo Heavy Industry Accelerator Service Ltd. for operation of the cyclotron and Kiyoshi Kyono, Emi Hayashinaka, and Keiji Noutomi of the RIKEN Center for Molecular Imaging Science for the expert technical assistance. We also express our great appreciation to Boehringer Ingelheim Pharma KG for providing us *N*-desmethyl telmisartan (BIBT9584).

REFERENCES

(1) Stangier, J.; Schmid, J.; Turck, D.; Switek, H.; Verhagen, A.; Peeters, P. A.; van Marle, S. P.; Tamminga, W. J.; Sollie, F. A.; Jonkman, J. H. Absorption, metabolism, and excretion of intravenously and orally administered [14C]telmisartan in healthy volunteers. *J. Clin. Pharmacol.* **2000**, *40* (12 Part 1), 1312–22.

(2) Stangier, J.; Su, C. A.; Schondorfer, G.; Roth, W. Pharmacokinetics and safety of intravenous and oral telmisartan 20 mg and 120 mg in subjects with hepatic impairment compared with healthy volunteers. *J. Clin. Pharmacol.* **2000**, *40* (12 Part 1), 1355–64.

(3) Wienen, W. E., M.; van Meel, J. C. A.; Stangier, J.; Busch, U.; Ebner, T.; Schmid, J.; Lehmann, H.; Matzek, K.; Kempthorne-Rawson, J.; Gladigau, V.; Hauel, N. H. A review on Telmisartan: A Novel, Long-Acting Angiotensin II-Receptor Antagonist. *Cardiovasc. Drug Rev.* **2000**, *18* (2), 127–154.

(4) Nishino, A.; Kato, Y.; Igarashi, T.; Sugiyama, Y. Both cMOAT/MRP2 and another unknown transporter(s) are responsible for the biliary excretion of glucuronide conjugate of the nonpeptide angiotensin II antagonist, telmisaltan. *Drug Metab. Dispos.* **2000**, *28* (10), 1146–8.

(5) Ishiguro, N.; Maeda, K.; Kishimoto, W.; Saito, A.; Harada, A.; Ebner, T.; Roth, W.; Igarashi, T.; Sugiyama, Y. Predominant contribution of OATP1B3 to the hepatic uptake of telmisartan, an angiotensin II receptor antagonist, in humans. *Drug Metab. Dispos.* **2006**, *34* (7), 1109–15.

(6) Ishiguro, N.; Maeda, K.; Saito, A.; Kishimoto, W.; Matsushima, S.; Ebner, T.; Roth, W.; Igarashi, T.; Sugiyama, Y. Establishment of a set of double transfectants coexpressing organic anion transporting polypeptide 1B3 and hepatic efflux transporters for the characterization of the hepatobiliary transport of telmisartan acylglucuronide. *Drug Metab. Dispos.* **2008**, *36* (4), 796–805.

(7) Hagenbuch, B.; Meier, P. J. The superfamily of organic anion transporting polypeptides. *Biochim. Biophys. Acta* **2003**, *1609* (1), 1–18.

(8) Vavricka, S. R.; Van Montfoort, J.; Ha, H. R.; Meier, P. J.; Fattinger, K. Interactions of rifamycin SV and rifampicin with organic anion uptake systems of human liver. *Hepatology* **2002**, *36* (1), 164–72.

(9) Hirano, M.; Maeda, K.; Shitara, Y.; Sugiyama, Y. Drug-drug interaction between pitavastatin and various drugs via OATP1B1. *Drug Metab. Dispos.* **2006**, *34* (7), 1229–36.

(10) Kiyotani, K.; Mushiroda, T.; Kubo, M.; Zembutsu, H.; Sugiyama, Y.; Nakamura, Y. Association of genetic polymorphisms in SLCO1B3 and ABCC2 with docetaxel-induced leukopenia. *Cancer Sci.* **2008**, *99* (5), 967–72.

(11) Kusuhara, H.; Sugiyama, Y. In vitro-in vivo extrapolation of transporter-mediated clearance in the liver and kidney. *Drug Metab. Pharmacokinet.* **2009**, *24* (1), 37–52.

(12) Watanabe, T.; Maeda, K.; Kondo, T.; Nakayama, H.; Horita, S.; Kusuhara, H.; Sugiyama, Y. Prediction of the hepatic and renal clearance of transporter substrates in rats using in vitro uptake experiments. *Drug Metab. Dispos.* **2009**, *37* (7), 1471–9.

(13) Watanabe, T.; Kusuhara, H.; Maeda, K.; Shitara, Y.; Sugiyama, Y. Physiologically based pharmacokinetic modeling to predict transporter-mediated clearance and distribution of pravastatin in humans. *J. Pharmacol. Exp. Ther.* **2009**, *328* (2), 652–62.

(14) Watanabe, T.; Kusuhara, H.; Maeda, K.; Kanamaru, H.; Saito, Y.; Hu, Z.; Sugiyama, Y. Investigation of the rate-determining process in the hepatic elimination of HMG-CoA reductase inhibitors in rats and humans. *Drug Metab. Dispos.* **2010**, *38* (2), 215–22.

(15) Takashima, T.; Nagata, H.; Nakae, T.; Cui, Y.; Wada, Y.; Kitamura, S.; Doi, H.; Suzuki, M.; Maeda, K.; Kusuhara, H.; Sugiyama, Y.; Watanabe, Y. Positron Emission Tomography Studies Using (15R)-16-m-[11C]tolyl-17,18,19,20-tetranorisocarbacyclin Methyl Ester for the Evaluation of Hepatobiliary Transport. *J. Pharmacol. Exp. Ther.* **2010**, *335* (2), 314–23.

(16) Kim, D. C.; Sugiyama, Y.; Satoh, H.; Fuwa, T.; Iga, T.; Hanano, M. Kinetic analysis of in vivo receptor-dependent binding of human epidermal growth factor by rat tissues. *J. Pharm. Sci.* **1988**, *77* (3), 200–7.

(17) Ebner, T.; Heinzel, G.; Prox, A.; Beschke, K.; Wachsmuth, H. Disposition and chemical stability of telmisartan 1-O-acylglucuronide. *Drug Metab. Dispos.* **1999**, *27* (10), 1143–9.

(18) Davies, B.; Morris, T. Physiological parameters in laboratory animals and humans. *Pharm. Res.* **1993**, *10* (7), 1093–5.

(19) Everett, N. B.; Simmons, B.; Lasher, E. P. Distribution of blood (Fe 59) and plasma (I 131) volumes of rats determined by liquid nitrogen freezing. *Circ. Res.* **1956**, *4* (4), 419–24.

(20) Niemi, M.; Backman, J. T.; Fromm, M. F.; Neuvonen, P. J.; Kivisto, K. T. Pharmacokinetic interactions with rifampicin: clinical relevance. *Clin. Pharmacokinet.* **2003**, *42* (9), 819–50.

(21) Schuetz, E. G.; Schinkel, A. H.; Relling, M. V.; Schuetz, J. D. P-glycoprotein: a major determinant of rifampicin-inducible expression of cytochrome P4503A in mice and humans. *Proc. Natl. Acad. Sci. U.S.A.* **1996**, *93* (9), 4001–5.

(22) Fromm, M. F.; Kauffmann, H. M.; Fritz, P.; Burk, O.; Kroemer, H. K.; Warzok, R. W.; Eichelbaum, M.; Siegmund, W.; Schrenk, D. The effect of rifampin treatment on intestinal expression of human MRP transporters. *Am. J. Pathol.* **2000**, *157* (5), 1575–80.

(23) Lau, Y. Y.; Huang, Y.; Frassetto, L.; Benet, L. Z. effect of OATP1B transporter inhibition on the pharmacokinetics of atorvastatin in healthy volunteers. *Clin. Pharmacol. Ther.* **2007**, *81* (2), 194–204.

(24) Thummel, K. E.; Shen, D. D.; Isoherranen, N.; Smith, H. E. Design and Optimization of Dosage Regimens: Pharmacokinetic Data. In *The Pharmacological Basis of Therapeutics*, 11th ed.; Gilman, A. G., Goodman, L. S., Laurence, L. B., John, S. L., Keith, L. P., Eds.; McGraw-Hill Publishing Co.: New York, 2006; pp 1787−888.

(25) Fattinger, K.; Cattori, V.; Hagenbuch, B.; Meier, P. J.; Stieger, B. Rifamycin SV and rifampicin exhibit differential inhibition of the hepatic rat organic anion transporting polypeptides, Oatp1 and Oatp2. *Hepatology* **2000**, *32* (1), 82–6.

(26) Lau, Y. Y.; Okochi, H.; Huang, Y.; Benet, L. Z. Multiple transporters affect the disposition of atorvastatin and its two active hydroxy metabolites: application of in vitro and ex situ systems. *J. Pharmacol. Exp. Ther.* **2006**, *316* (2), 762–71.

(27) Shitara, Y.; Sugiyama, D.; Kusuhara, H.; Kato, Y.; Abe, T.; Meier, P. J.; Itoh, T.; Sugiyama, Y. Comparative inhibitory effects of different compounds on rat oatpl (slc21a1)- and Oatp2 (Slc21a5)-mediated transport. *Pharm. Res.* **2002**, *19* (2), 147–53.

(28) Ueda, K.; Kato, Y.; Komatsu, K.; Sugiyama, Y. Inhibition of biliary excretion of methotrexate by probenecid in rats: quantitative prediction of interaction from in vitro data. *J. Pharmacol. Exp. Ther.* **2001**, *297* (3), 1036–43.

(29) Kitamura, Y.; Hirouchi, M.; Kusuhara, H.; Schuetz, J. D.; Sugiyama, Y. Increasing systemic exposure of methotrexate by active efflux mediated by multidrug resistance-associated protein 3 (mrp3/abcc3). *J. Pharmacol. Exp. Ther.* **2008**, *327* (2), 465–73.

(30) Leonhardt, M.; Keiser, M.; Oswald, S.; Kuhn, J.; Jia, J.; Grube, M.; Kroemer, H. K.; Siegmund, W.; Weitschies, W. Hepatic uptake of the magnetic resonance imaging contrast agent Gd-EOB-DTPA: role of human organic anion transporters. *Drug Metab. Dispos.* **2010**, *38* (7), 1024–8.

(31) Ghibellini, G.; Leslie, E. M.; Pollack, G. M.; Brouwer, K. L. Use of tc-99m mebrofenin as a clinical probe to assess altered hepatobiliary transport: integration of in vitro, pharmacokinetic modeling, and simulation studies. *Pharm. Res.* **2008**, *25* (8), 1851–60.

(32) Swift, B.; Yue, W.; Brouwer, K. L. Evaluation of (99m)technetium-mebrofenin and (99m)technetium-sestamibi as specific probes for hepatic transport protein function in rat and human hepatocytes. *Pharm. Res.* **2010**, *27* (9), 1987–98.

(33) Combes, R. D.; Berridge, T.; Connelly, J.; Eve, M. D.; Garner, R. C.; Toon, S.; Wilcox, P. Early microdose drug studies in human volunteers can minimise animal testing: Proceedings of a workshop organised by Volunteers in Research and Testing. *Eur. J. Pharm. Sci.* **2003**, *19* (1), 1–11.